Gopidi *et al. J. Mater. Inf.* **2025**, *5*, 19
DOI: 10.20517/jmi.2024.41

Journal of Materials Informatics

Research Article

Open Access

Check for updates

Unveiling defect physics in gapped metals: a theoretical investigation into defect formation and electronic structure interplay

Harshan Reddy Gopidi[1], Lovelesh Vashist[1], Oleksandr I. Malyi[1,2,*]

[1]Centre of Excellence ENSEMBLE3 Sp. z o. o., Warsaw 01-919, Poland.
[2]Qingyuan Innovation Laboratory, Quanzhou 362801, Fujian, China.

[*]**Correspondence to:** Dr. Oleksandr I. Malyi, Qingyuan Innovation Laboratory, 1 Xueyuan Rd, Quanzhou 362801, Fujian, China. E-mail: oleksnadrmayi@gmail.com

How to cite this article: Gopidi, H. R.; Vashist, L.; Malyi, O. I. Unveiling defect physics in gapped metals: a theoretical investigation into defect formation and electronic structure interplay. *J. Mater. Inf.* **2025**, *5*, 19. https://dx.doi.org/10.20517/jmi.2024.41

Received: 31 Aug 2024 **First Decision:** 22 Nov 2024 **Revised:** 26 Dec 2024 **Accepted:** 3 Jan 2025 **Published:** 3 Mar 2025

Academic Editor: Xiang-Dong Ding **Copy Editor:** Ting-Ting Hu **Production Editor:** Ting-Ting Hu

Abstract

In materials science, point defects play a crucial role in materials properties. This is particularly well known for the wide band gap insulators where the defect formation/compensation determines the equilibrium Fermi level and generally the doping response of a given material. Similarly, the main defect trends are also widely understood for regular metals (e.g., Cu and Zn discussed herein). With the development of electronic structure theory, a unique class of quantum materials - gapped metals (e.g., $Ca_6Al_7O_{16}$, $SrNbO_3$, $In_{15}SnO_{24}$, and CaN_2) that exhibit characteristics of both metals and insulators - has been identified. While these materials have internal band gaps similar to insulators, their Fermi level is within one of the main band edges, giving a large intrinsic free carrier concentration. Such unique electronic structures give rise to unusual defect physics, e.g., when the acceptor defect formation in n-type gapped metal results in the decay of the conducting electron to the acceptor states. In concentration limits, such electron-hole recombination can compensate for the energy needed to break chemical bonds and form acceptor vacancy, often leading to off-stoichiometric compounds. Such unusual physics, however, makes these quantum materials distinct from traditional compounds. Motivated by this, herein, we establish a minimal level of theory needed to account for the complex interplay between electronic structure and analyzing defects in gapped metals that can be utilized for their design in different practical applications.

Keywords: Materials science, gapped metals, defects, electronic structure theory

INTRODUCTION

Every material contains point defects occurring as the result of an interplay between the energy cost to introduce change in local bonding environments and an increase in configuration entropy[1-3]. While point defects can be considered as imperfections of the solids, it turns out that they often define materials properties. This is especially well noted for insulators where defect compensation defines the position of the equilibrium Fermi level[4-10], the n- and p-type nature of a compound[6,11], and even the doping response of a solid[4,6,9,12]. For instance, the majority of the oxides (e.g., ZnO) cannot be made p-type due to the low position of the principal valence band maximum[13-15]. This led the research community to use the electronic structure theory as a common tool to investigate defect physics, forming the concept of defect transition levels, n- and p-type pinning energy[11], H pinning energy[14,15], or even more generally that formation (concentration) of point defect is defined not only by the defect itself but by other defects via accounting for the charge neutrality rule[16]. Hence, modern experimental methodologies, such as atomic-resolution transmission electron microscopy, scanning tunneling microscopy, positron annihilation spectroscopy, deep-level transient spectroscopy, and electron paramagnetic resonance, are extensively employed to elucidate, detect, and scrutinize defects with high accuracy. These techniques are particularly potent when synergized with density functional theory (DFT) analysis of point defects that often can provide vital details on specific defect properties (e.g., transition levels)[17].

Within the defect theory, the main idea of DFT calculations is to use small simulation cells and reproduce properties of defects in the dilute limit. However, it becomes clear that the description of the formation energy of point defects can directly be affected by simulation cells. Thus, periodic boundary conditions can influence the behavior of defects in several significant ways: (i) defect can induce artificial interaction due to defect-induced local strain[18,19]; (ii) supercell with charge defects has strong charge-charge interaction[20-23]; (iii) adding electrons or holes to the system can result in artificial band filling when for instance instead of occupation of the bottom of conduction band the carrier addition results in occupation band within non-negligible energy range[24]. It is worth noting that the inaccuracies brought about by these finite-size effects can have profound consequences for the interpretation of physical results and the understanding of potential practical applications of the proposed materials. We emphasize that all the above size effects come from the small supercell size and, in principle, can be avoided by scaling defect formation energy with supercell size[25-27] or applying specific post-energy corrections[20,24,26,28-30]. Indeed, the power of both approaches has been demonstrated for a number of insulators in understanding experimental results - researchers have been able to unravel the microscopic mechanisms governing defect behavior[31-33], color centers[34-36], and other crucial processes within insulators[6,11].

In traditional insulators, the accurate depiction of defects typically necessitates a comprehensive approach that includes various corrections and the use of an exchange-correlation functional capable of precisely replicating band gap energy, as done in relevant literature [25,26,37]. In the case of metal, however, the common beliefs are different: (i) one needs to minimize the strain interaction between defects with sufficiently large supercell size; (ii) there are no charged defects in metals as in contrast to a defect-dependent definition of Fermi level in insulators; Fermi level in metal is directly calculated from a number of free carriers - i.e., adding or removing an electron from the system result not in the formation of charge defect but adding or removing electrons to Fermi level[38]; (iii) band filling correction is explicitly not accounted because of continuous nature of bands in metals. Because of this, it is common that there is no post-process correction used in calculations of defect formation energy in metals as long as the supercell size in each direction is larger than about 10 Å to minimize indirect interaction between the defect and its periodic images. Keeping this in mind, herein, we revisit the defect physics in metallic compounds, showing, for instance, that not all metals are alike. Importantly, we demonstrate new defect physics in a new type of quantum materials -

gapped metals, which show a complex interplay between their electronic structure and defect formation; in this way, we establish a theoretical foundation for analyzing defects in this new type of quantum materials explaining, in particular, the role of band filling correction in the accurate calculations of defect formation energy. These results, while focusing primarily on a fundamental understanding of defect physics, also offer significant practical applications by explaining the basic methodological aspects. Specifically, the work explains, how defect formation results in the decay of conducting electrons into the acceptor states, thereby reducing the defect formation energy and indicating possible reasons for off-stoichiometry of gapped metals[38-42]. Historically, the formation of off-stoichiometric compounds has often been attributed to growth effects. However, the physics discussed here reveals that the interplay between electronic properties and defect formation can drive the formation of off-stoichiometric compounds as an intrinsic tendency of the system, independent of growth effects. Moreover, taking into account that in electronic structure theory, defect formation energy is the fundamental property used to define equilibrium Fermi level[4-10], defect transition level[14,15,17,43], optical properties[44], or the general doping tendency of the system[16], the discussed methodological aspects in defect calculations explain thus a minimal level of theory needed to account for unique defect physics in gapped metals accurately.

MATERIALS AND METHODS

All calculations were performed using the Vienna Ab initio Simulation Package (VASP)[45-48], employing the Perdew-Burke-Ernzerhof (PBE)[49] functional. For plane wave basis, the cutoff energy levels were set to 550 eV for volume relaxation, and for structural relaxation, the default values were used. The atomic relaxations were carried out (unless otherwise specified) until the intrinsic forces were below 0.01 eV/Å. The Γ-centered Monkhorst-Pack k-grid with a density of 10,000 per reciprocal atom was utilized for all main calculations (minimum k-points 2×2×2). This k-point density is usually more than sufficient for the calculations of defect properties, as, for instance, has been discussed in our previous works.[24] The results were analyzed using pymatgen[50] and Vesta[51]. For regular metals, we used Cu (SG: 225)[52] and Zn (SG: 194)[53] as representative examples. While for the gapped metals, the calculations were performed for $SrNbO_3$ (SG: 62)[54], $Ca_6Al_7O_{16}$ (SG: 220)[55], CaN_2 (SG: 139)[56], and $In_{15}SnO_{24}$ (SG: 148)[57]. The details on crystal structures are given in Supplementary Materials. For the simplicity of the discussed physics, we focused on cation vacancies (acceptor defects in the case of n-type gapped metals) in the gapped metals, as they are known to be the most common types of defects in these compounds and play a significant role in optical properties[38,39]. The conclusions discussed herein, however, are fully expected to work for other types of systems, including donor defects. The electronic band structures were computed using the corresponding primitive zone and k-path Brillouin zone mapping from Ref.[58].

For a given material, to understand the defect properties in the dilute limit, the vacancy formation energy (ΔH) was calculated as:

$$\Delta \mathrm{H} = E_{S+V} - E_S + \mu_A^0 + \Delta\mu_A + E_{corr} \quad (1)$$

where E_{S+V}, E_S, μ_A^0, $\Delta\mu_A$, and E_{corr} are the energy of the supercell containing defect, energy of perfect supercell, elemental chemical potential, relative chemical potential, and energy correction due to finite supercell size, respectively. It should, however, be noted that PBE calculations are known to result in band gap underestimation[59], which, in some semiconductors/insulators, is known to reduce the accuracy of the defect formation energy calculations[10,60]. This dependence is considered significantly less critical for metallic compounds[61]. Taking this and the focus of this work into account, herein, we present relative defect formation energy (e.g., difference of ΔH for different supercell sizes) unless otherwise specified.

RESULTS AND DISCUSSION

Not all metals are alike and strong size-dependent defect formation energy is possible

In traditional metals, the formation energy of point defects [Figure 1A] is weakly dependent on supercell size after reaching separation of the point defects around 10 Å, which is indeed in good agreement with our first-principles calculations for Cu (SG: 225) and Zn (SG: 194) systems shown in Figure 1B. This behavior is not surprising as metals typically have more delocalized electron distributions and can easily accommodate strains due to their malleability as compared to regular insulators (e.g., ZnO). Moreover, the free electrons can screen long-range interactions when, for instance, a charge is introduced to the system. This electronic screening is much weaker in insulators due to the lower dielectric constant. As a result, the defect formation energy in metals tends to be less sensitive to supercell size. We note, however, that herein, we find that for some metals, defect formation energy has strong supercell size dependence. For instance, in Figure 1B, we demonstrate that for some metals, the change in defect formation with supercell size is significant even when the effective lateral dimension of the system is larger than 10 Å. For instance, for $Ca_6Al_7O_{16}$ (SG: 220), the Al vacancy formation energy (calculated without accounting for any corrections, Figure 1A and B) for 58 and 464-atom supercells differs by 3.14 eV. Similar behavior is observed for $SrNbO_3$:V_{Nb}, $In_{15}SnO_{24}$:V_{In}, and CaN_2:V_{Ca} (see details on the dataset of used materials in methods).

Size dependence of defect formation energy does not originate from structural changes within different supercells or interaction of localized states

One may naively think that a change in defect formation energy is coming due to a change of internal structure - i.e., depending on supercell size different local structural displacements are stabilized and one needs significantly large supercell size to converge such structural distortion. However, the change of defect formation energy in order of couple eV is significantly larger than that observed for typical defect relaxation[18,19]. To demonstrate this, we analyze atomic displacement in the first coordination sphere for different supercell sizes [Figure 2A and B]. The results show that with increasing supercell size, the relative atomic displacements converge. Here, it should be noted that for most of the systems starting slightly above 10 Å (except the $SrNbO_3$:V_{Nb}), all atomic displacements are close to the approximate values. Importantly, a comparison of the results between Figure 1B and Figure 2B demonstrates that the convergence of structural properties is reached significantly faster than the convergence of defect formation energy. For instance, increasing the supercell size from 160 to 320 atoms for $In_{15}SnO_{24}$:V_{In} results only in a difference in relative relaxation for the first coordination sphere of ~0.006 Å, while the corresponding change in defect formation energy is 0.57 eV. These results thus imply that while the convergence of internal atomic displacements can result in a change of defect formation energy[18], it does not appear to be the driving force for the supercell size dependence of defect formation energy in the considered metals.

Gapped metals as a unique class of quantum materials

To understand better the possible origin for the size dependence of defect formation energy, we refer to the electronic structures [Figure 3] of the different metallic compounds shown in Figure 1B (the band structure results presented herein are in good agreement with corresponding electronic structures shows in Materials Project[62]). We see that all metals have similar electronic properties with the presence of free carriers. What makes the substantial difference, however, is that in Cu and Zn, the Fermi level crosses the part of the continuous band [Figure 3A and B] containing all valence electrons with pseudo-core states located significantly below it. In contrast, $SrNbO_3$, $In_{15}SnO_{24}$, $Ca_6Al_7O_{16}$, and CaN_2 also have free carriers, but the Fermi level is not located in the continuous region of the band structure as seen in Cu and Zn cases. These compounds are known as gapped metals[38,63,64] - a unique class of quantum materials superposing the existence of a large internal band gap and Fermi level inside of one of the principal band edges. Thus, $SrNbO_3$, $In_{15}SnO_{24}$, and CaN_2 are n-type gapped metals having Fermi levels inside of the principal conduction band and a large internal band gap below it [Figure 3C, D and F]. At the same time, $Ca_6Al_7O_{16}$ is an intermediate band gap compound with a partially occupied band [Figure 3E], for simplicity of further

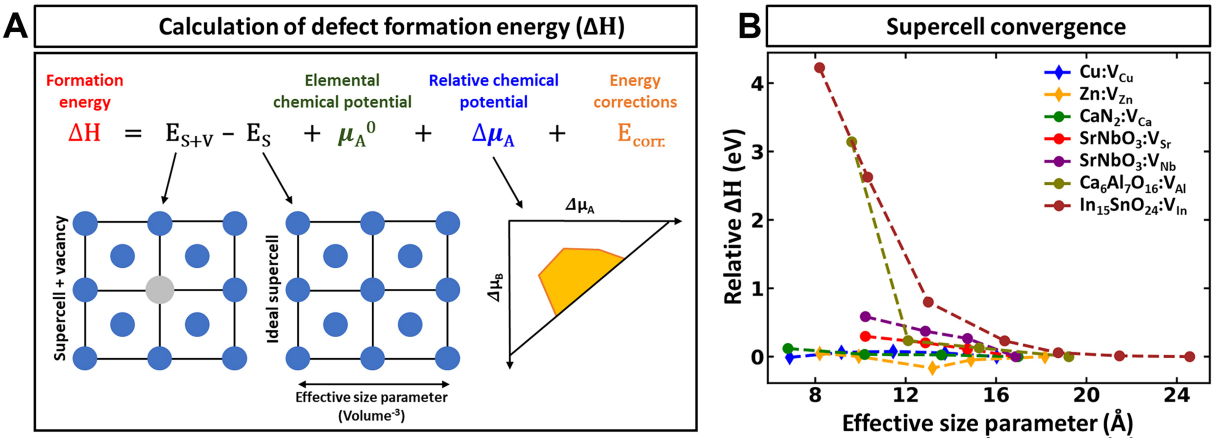

Figure 1. Calculation of defect formation energy for different metals. (A) Schematic for calculations of defect formation energy for metals for different supercell sizes; (B) Relative defect formation energy calculated as the difference of defect formation energy for a given supercell and that for the largest supercell considered for a given system. The figure (A) is inspired by Ref.[29].

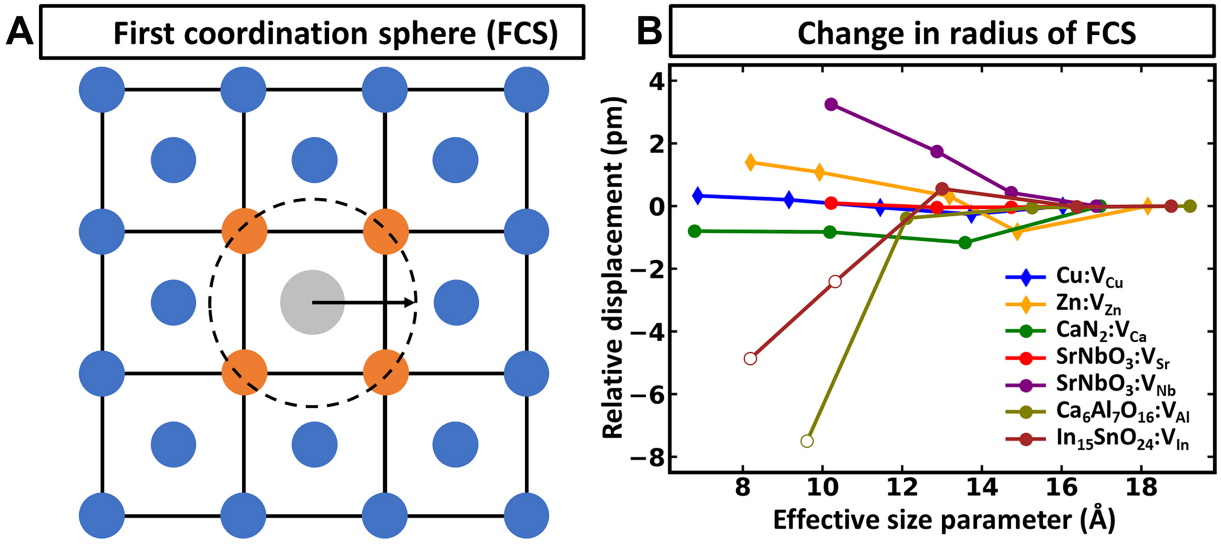

Figure 2. Defect-induced displacements in metals. (A) Schematic illustration of the distribution of local neighbors around the vacancy site showing the first coordination sphere; (B) Relative atomic displacement with respect to supercell size for different metals (hollow circles indicate a system where defect formation removes all free carriers from the principal conduction band). Relative displacement is calculated with respect to the displacement in the largest supercell for each system.

discussion, we will also refer to this compound as n-type gapped metal. We note that all these compounds belong to a wide family of materials that recently attracted significant attention as potential electrides[65-68], thermoelectrics[64,69], and transparent conductors[38,63,70-72]. These thus suggest that while gapped metals have metallic properties (e.g., increased resistivity with temperature), they also have inherent properties for insulators (e.g., presence of an internal gap between principal band edges). Moreover, in these compounds, only a fraction of valence electrons contributes to free carrier concentration. For instance, $SrNbO_3$ has 1e per formula unit in the principal conduction band with an internal band gap energy of 2.5 eV. Indeed, for all these compounds, the free carrier concentration can be estimated using the sum of composition-weighted common oxidation states (e.g., in the case of $SrNbO_3$, the common oxidation states are +2, +5, and -2 for Sr, Nb, and O, respectively; it should also be noted that the physical meaning of the oxidation state

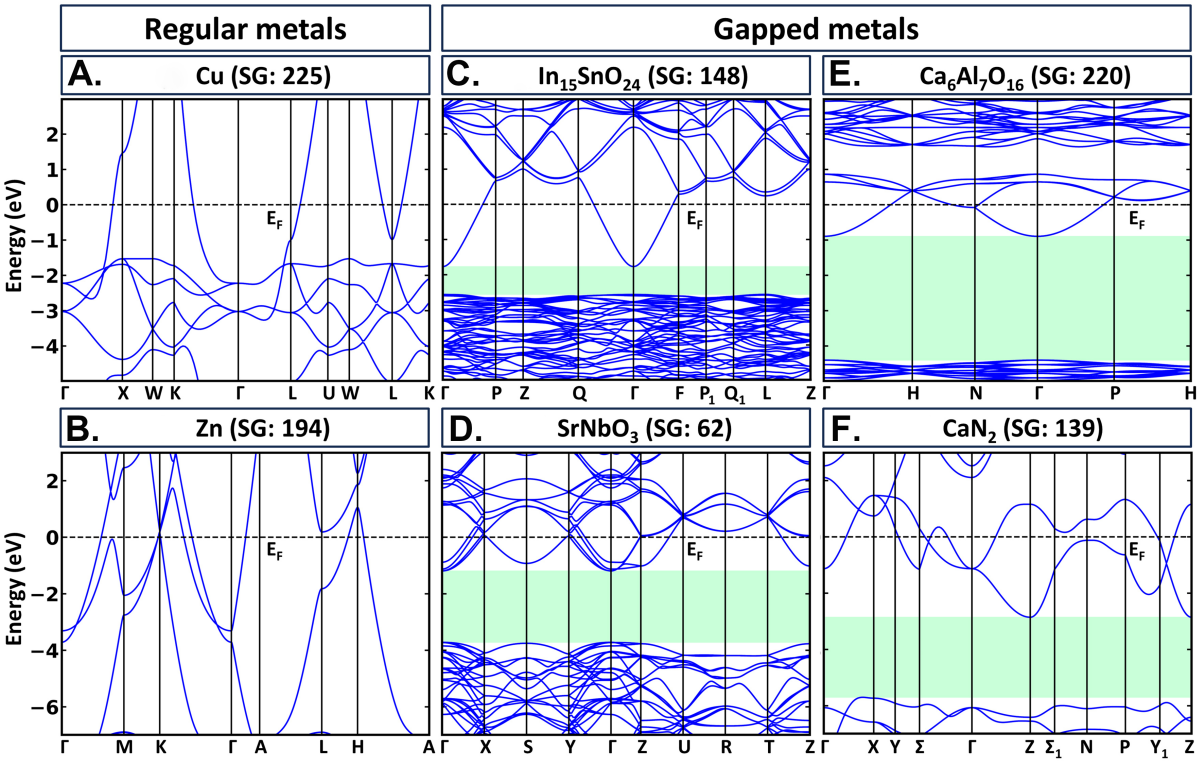

Figure 3. Electronic properties of different types of metals. Electronic band structures of (A and B) regular metals and (C-E) gapped metals as computed using PBE exchange-correlation functional. The space group number is abbreviated as SG. E_F is the Fermi level. The internal band gap for gapped metals is shown as the shaded green region. PBE: Perdew-Burke-Ernzerhof; SG: space group.

should not be confused with the partial charges on each atom, as explained in Refs.[73,74]). The electronic structure of such gapped metal thus resembles that of degenerate semiconductors (e.g., wide-band gap insulators heavily doped by n- or p-type elements) with the main difference lying, in fact, that gapped metals are usually stable (with respect to decomposition to competing phases) intrinsic compounds obtained without any intentional doping and having significantly large free carrier concentration as compared to that for degenerate semiconductors.

The electronic structure of gapped metal has unique consequences on defect physics

In conventional metals such as Cu and Zn, the formation of a vacancy occurs when an atom is removed, thus leaving a "void" in the lattice structure. This void can be occupied by an electron from the "electron sea". Moreover, in these metals, all atoms are structurally equivalent. Hence, the generation of a vacancy leads to the removal of both the associated electrons and their corresponding energy states from the electronic configuration, resulting in no significant change in the Fermi level. On the other hand, with gapped metals, vacancy formation, such as that of an acceptor, can lead to pronounced changes in electronic properties. This is because the newly-formed acceptor state introduces unoccupied states (as schematically shown in Figure 4A) below the Fermi level, which can cause some conductive electrons to move from the main conduction band to the acceptor level (a similar mechanism also exists for p-type gapped metals - i.e., compounds having a Fermi level in the principal valence band and a large internal band gap above it[75,76]). This shift can lead to a significant change in carrier concentration, especially in small supercells. For instance, in $SrNbO_3$, a single Nb vacancy removes 5e per vacancy from the principal conduction band. Similar effects are noted in other gapped metals. Specifically, Ca vacancy in CaN_2 removes 2e, Al vacancy in $Ca_6Al_7O_{16}$ removes 3e, and In vacancy in $In_{15}SnO_{24}$ removes 3e from the principal conduction band. While

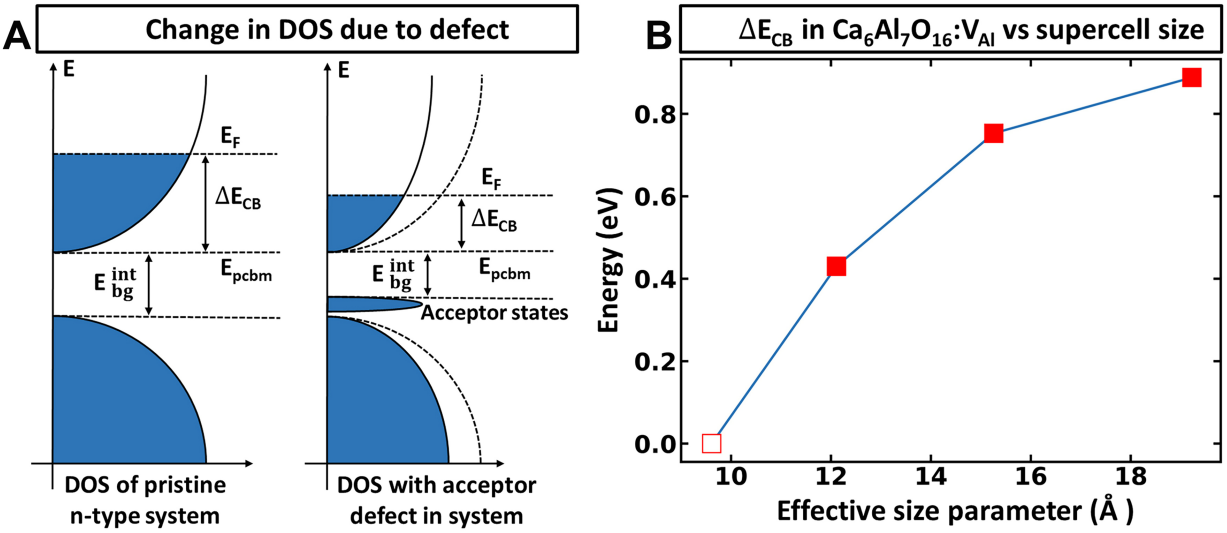

Figure 4. Effect of acceptor defect formation on electronic properties of gapped metals. (A) Schematic illustration of the electronic structure of n-type gapped metal for pristine and acceptor defect systems (where E_{bg}^{int} is the internal band gap, E_{pcbm} is the principal conduction band minimum, E_F is the Fermi level and E_{CB} is the occupied conduction band width defined as E_F-E_{pcbm}); (B) E_{CB} *vs.* supercell size in $Ca_6Al_7O_{16}$:V_{Al} system containing single Al vacancy (hollow square is when all electrons are completely removed from principal conduction band). DOS: Density of states.

these results may be fully visible in the case of high concentration (which indeed can be realized in some gapped metals[38,76-78]), this behavior implies that an accurate description of defect formation energy at a dilute regime should account for a reduction of free carrier concentration. For instance, in Figure 4B, one can see how the defect formation results in a change of the occupied part of the principal conduction band (ΔE_{CB}) in $Ca_6Al_7O_{16}$. Thus, the formation of Al vacancy in a 116-atom supercell reduces ΔE_{CB} to 0.43 eV, while the corresponding ΔE_{CB} for a 464-atom supercell is 0.89 eV. In the case of certain supercells, the creation of vacancies may lead to a transition from metal to insulator or even a shift of the Fermi level from the principal conduction band to the principal valence band, as exemplified in Figure 2B and Figure 4B. This is akin to the behavior seen in insulators where the formation of donor or acceptor defects induces occupation in the conduction or valence band over an artificially wide energy range, differing only in gapped metals where the reference state already has Fermi level in one of the principal band edges. The change of the occupied part of the conduction band as the function of the supercell size directly correlates to defect energetics, as the energy levels of occupied states are integral to the extension of DFT energy, indicating that each alteration in occupation seen across different supercells will directly influence the defect formation energy. Moreover, for a given compound, a larger shift in the Fermi level due to defect formation results in a larger change of defect formation energy. These results thus can be understood in the following way - the formation of acceptor vacancy in the n-type gapped metal leads to the formation of the unoccupied acceptor level below the Fermi level, resulting in the decay of conducting electrons to the acceptor level. A larger concentration of acceptor defects leads to more free carrier removal for the principal conduction band. Notably, the decay of conducting electrons also implies that vacancy formation not only leads to breaking chemical bonds but also can benefit from the reduction of internal energy by moving electrons from high energy to low energy acceptor levels. Because of this, for a range of experimental conditions, energy lowering due to electron decay can offset the energy cost to break chemical bonds, leading to the formation of off-stoichiometric gapped metals[38-42]. While the above discussion is given for the case of the acceptor formation in n-type gapped metals, the physics discussed herein can also be extended to other systems. For instance, in the case of p-type gapped metals (i.e., compounds having Fermi level in the principal valence band and large internal band gap above it), the formation of donor defect can

result in a change of occupation of the principal valence band, which in a specific situation can lead to the formation of the off-stoichiometric compound (e.g., as discussed for Ba_4As_{3-x})[76,79].

Physics of band-filling correction in gapped metals and other factors that can affect calculations of defect formation energy

One may wonder what the impact of the electronic properties on the supercell-size dependence of defect formation energy is. In traditional insulators, the problem of band-filling is usually solved using either the supercell scaling (it should be noted that scaling is usually done to account for all factors at the same time and is not specific for band filling) or applying post-process band-filling correction (BFC)[24,26]. In the case of the scaling approach, the defect formation energy for the range of supercells is extrapolated to the dilute limit based on the guess of potential physical phenomena controlling the process. In the BFC scheme, the main idea is to restore the expected occupation corresponding to the dilute limit; i.e., in gapped metals, defect formation should not affect the Fermi level in the dilute limit. This expected energy correction thus can be calculated by summation over the eigenvalues as:

$$\Delta_{BFC} = -\Sigma_{n,k}[\Theta(e_{n,k} - E_F)\omega_k\gamma_{n,k}(e_{n,k} - E_F) + \Theta(E_F - e_{n,k})(\omega_k(1 - \gamma_{n,k})(E_F - e_{n,k})] \quad (2)$$

where $\Theta(X)$ is the Heaviside step function, ω_k are the weights of the k-points, $e_{n,k}$ are the eigenenergies of state (n, k), $\gamma_{n,k}$ are the occupations of the eigenstate (n, k), and E_F is the Fermi level of the defect supercell with infinite volume (supercell without defects). We note, however, that, in practical scenarios, the emergence of point defects affects all eigenvalues[Figure 5A and B]. This is because plane-wave first-principles codes do not have common reference states for eigenvalues, and hence the BFC formalism indicated above cannot be straightforwardly employed unless a proper alignment of eigenvalues for both defective and pristine systems is made. To illustrate the complexity of such calculations, we consider the formation of Nb and Sr vacancies in the 160-atom $SrNbO_3$ supercell. As shown in [Figure 5A and B], both these defects are acceptors but remove different numbers of electrons from the principal conduction band. Specifically, Sr vacancy removes only 2e per vacancy from the conduction band, compared to 5e for the Nb case. The analysis of the electronic density of states shows that the defect formation changes the absolute eigenvalues for both systems compared to those for the pristine case. In our previous work[24], we demonstrated that one could use the electrostatic potentials at the cores of the most remote atoms to align the energy levels of pristine and defective systems and, in this way, efficiently describe the BFC in regular insulators such as ZnO. For gapped metals, such alignment is critical as small inaccuracies in its calculations can result in a noticeable change in defect formation energy due to the fact that the gapped metals have high free carrier concentration. To implement the alignment of eigenvalues between pristine and defective systems, we first identify the atoms located far from the defect, ensuring that these sites are minimally perturbed by the defect. We then extract the macroscopic average of the electrostatic potential and project it onto these chosen reference atoms. By comparing the electrostatic potentials of identical reference atoms in both pristine and defective supercells, we determine a shift that aligns the eigenvalues. Since different atomic species may experience the defect differently, we test the alignment using different atomic species. For instance, for $SrNbO_3$:Nb, potential alignment using electrostatic potentials for the most remote O *vs.* the most remote Nb atoms results in a difference in the relative defect formation energy of 0.17 eV for 160-atom supercell [Figure 5C]. As supercell size increases, the defect formation energies calculated for different methods of potential alignments approach each other[Figure 5D]. As noted above, the main cause for such behavior is different shifts of electrostatic potential for different atomic identities. Indeed, for some of the considered systems[Figure 6], there is no substantial difference in the results for different alignment methods. While a more detailed study is needed, we find that this behavior is observed for systems having distinct elemental contributions to band edges - for $SrNbO_3$, the principal conduction band is primarily dominated by Nb-d states, while the corresponding contributions from Sr and O are minimal. This thus

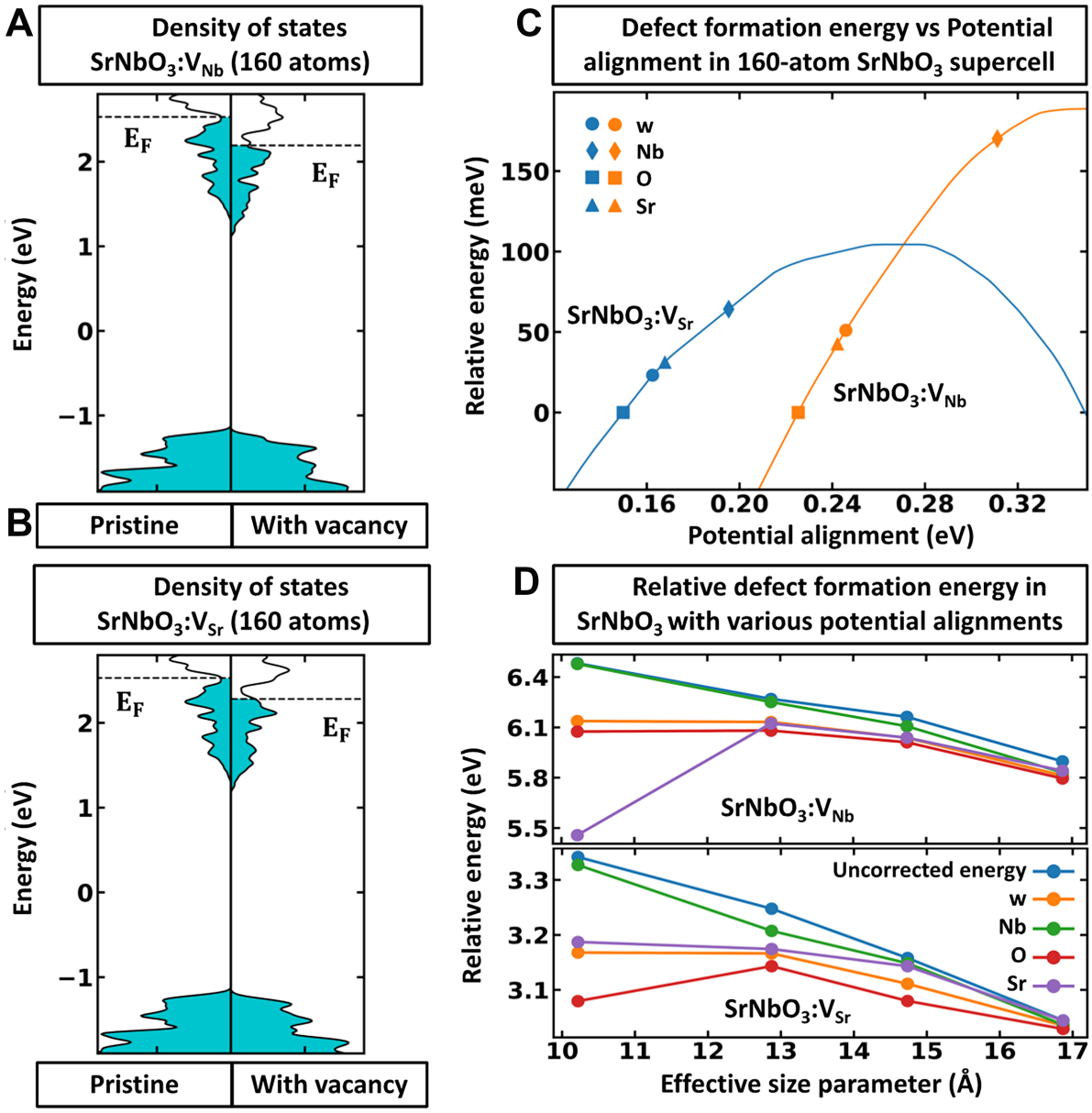

Figure 5. Strong dependence of defect formation energy on potential alignment. DOS for a 160-atom $SrNbO_3$ supercell is presented in two scenarios: (A) with and without Nb vacancy and (B) with and without Sr vacancy. These scenarios illustrate shifts in both the Fermi level and the eigenvalues. (C) Relative band filling correction *vs.* potential alignment, where Sr, Nb, O are averages over 3 most remote atoms of each kind and w is composition weighted average of Sr, Nb, and O potential alignments for 160-atom $SrNbO_3$ supercell containing Sr or Nb vacancy. For each system relative energies are with respect to corresponding O potential alignments. (D) Relative defect formation energy for Sr and Nb vacancy as a function of supercell size using different methods of potential alignment. Relative energy for each system is with respect to an arbitrary energy reference state. DOS: Density of states.

results in a fundamental question: what approach for band alignment should one choose for calculating defect formation energy?

To answer the above question, we recall that the main idea behind BFC is to mimic dilute limit in defect calculations. This practically means that for atoms located far away from the defect, the projected electronic structure should remain unaffected and that for most remote atoms, not only the position of the Fermi level

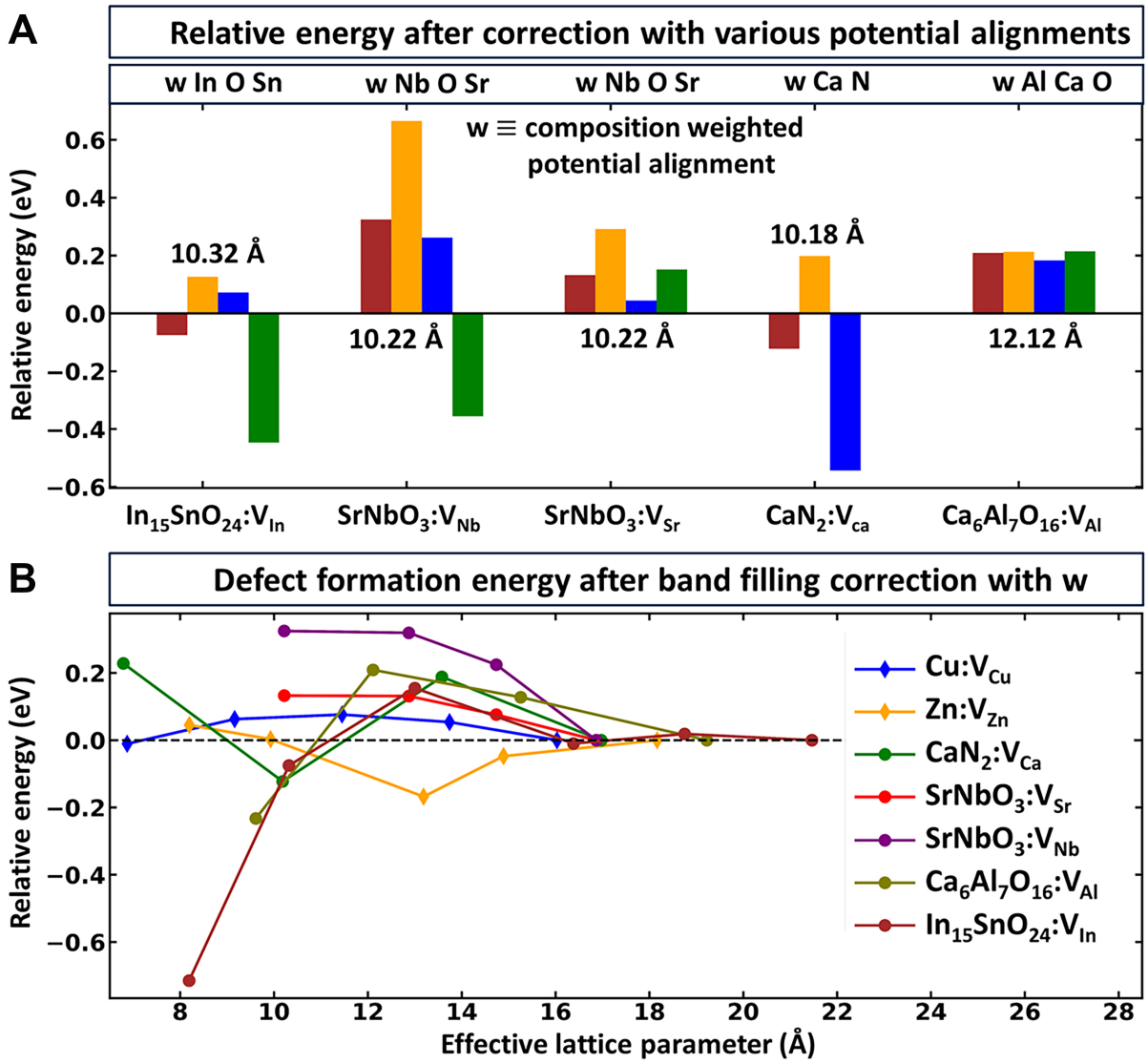

Figure 6. Corrected defect formation energy for gapped metals. (A) Relative defect formation energy with respect to largest supercell after accounting for band-filling correction energy using various methods for alignment of electrostatic potentials shown within the color scheme (average of 3 most remote atoms of each species and the composition weighed (w) potential alignment); (B) Defect formation energy after band filling correction with w alignment as a function of the size of the system. Relative energies in a and b are calculated with respect to the defect formation energy of the largest supercell after band-filling correction.

but also the position of band edges should remain unperturbed. Unfortunately, this behavior is often not fully achievable in supercell calculations. Because of this, herein, using a small dataset of gapped metals, we explored different ways for band alignment and identified that composition weighted average electrostatic potential for the most remote atoms from the defect provides the most consistent defect formation trends among different systems[Figure 6A and B]. The composition-weighted alignment can be motivated in the following way: change in the electrostatic potential of different atoms is different, and this results in the optimal change in the electrostatic potential for the entire system to be the composition-weighted average of the change in electrostatic potential of different atoms.

We note, however, that while it is crucial to incorporate BFCs for precise defect formation energy calculations in gapped metals, it is important to acknowledge other factors that may affect defect energetics. Thus, even in traditional metals, the defect formation energy is susceptible to variations in k-point density. Indeed, for Zn, for some supercells, the error bar is in the order of 0.1 eV as compared to converged defect formation energy sizes with ultra-dense k-point grid (i.e., 10,000 k-points per reciprocal atom *vs.* 100,000 k-points per reciprocal atom). For gapped metals, considered herein, this is a less critical factor, but for other gapped metals, it may play a more significant role. Furthermore, as noted above, defect formation can result in substantial relaxation (e.g., due to breaking strong anion-cation bonds) that may affect defect formation energy for some systems. For $SrNbO_3$:V_{Nb}, the difference in relaxation energy (i.e., computed as the energy difference of unrelaxed and relaxed systems containing the defect) computed for 80 and 360-atom supercells is 0.17 eV. Taking into account that relaxation energy is part of the total energy for a given system, it becomes obvious that verification of converging the atomic displacements as a function of supercell size is one of the critical steps that need to be accounted for in defect calculations.

CONCLUSIONS

In summary, using first-principles calculations, we provide a detailed analysis of defect formation in different gapped metals. We show that not all metals are similar to each other and demonstrate the unique defect physics of gapped metals (i.e., compounds having internal band gaps similar to insulators with Fermi level within one of the main band edges). For instance, while the formation energy of point defects in Cu and Zn (i.e., conventional metals) can be routinely calculated using relatively small-size supercells, gapped metals (i.e., quantum materials exemplified herein by $Ca_6Al_7O_{16}$, $SrNbO_3$, $In_{15}SnO_{24}$, and CaN_2) exhibit strong supercell size dependence of defect formation energy. This behavior is caused by the effect of point defects on their electronic structure. Thus, in n-type gapped metals - compounds having Fermi level inside the conduction band and a large internal band gap below it, the formation of an acceptor defect can result in a decay of a fraction of conducting electrons to the acceptor defect level (different relative fractions for different supercells), resulting in the reduction of free carrier concentration and shifting the Fermi level. For instance, for $SrNbO_3$, the formation of Nb vacancy removed 5 electrons per vacancy from the principal conduction band. While in the concentrated limit, such behavior reproduces the real behavior and can lead to the formation of non-stochiometric compounds (e.g., the formation of $Sr_{1-x}NbO_3$ is well experimentally known), to describe the defect formation energy in gapped metal in the dilute limit, one should explicitly account for the change of band filling and its effect on defect energetics, which indeed can be done, as we have demonstrated in this work, in the form of the post-process correction using potential alignment (here, composition weighted band alignment is found to most accurate for smallest supercell size) between defective and pristine systems made via utilizing composition-weighted alignment of electrostatic potential for most remote atoms. We emphasize as well that while including BFC is needed for describing the physics of gapped metals, other factors, such as converging internal relaxation, may also have a significant effect on accurate calculations of defect formation energy. In practical terms, our results show a significant difference in defect formation between regular materials (e.g., metals and insulators) and gapped metals, demonstrating the need for precise first-principles calculations to predict the properties of gapped metals accurately. While this study primarily addresses acceptor defects in n-type gapped metals, the methods are transferable to other systems and other types of defects. For example, the formation of donor defects in p-type gapped metals is also guided by the interplay of electron-hole recombination and change of band filling as the result of defect formation. This work thus provides a foundational methodological framework for future investigations into defect formation in any gapped metals.

DECLARATIONS

Authors' contributions

Data curation (lead), formal analysis (lead), investigation (lead), methodology (lead), validation (lead), writing - original draft (supporting): Gopidi, H.R.

Data curation (supporting), formal analysis (supporting), investigation (supporting), methodology (supporting), validation (supporting), writing - original draft (supporting): Vashist, L.

Data curation (supporting), formal analysis (supporting), investigation (supporting), methodology (supporting), validation (supporting), writing - original draft (lead), project administration (lead), supervision (lead): Malyi, O.I.

Availability of data and materials

The paper and Supplementary Materials provide the main data needed to reproduce the work. Additional data are available from the corresponding author upon reasonable request.

Financial support and sponsorship

The authors thank the "ENSEMBLE3 - Centre of Excellence for nanophotonics, advanced materials and novel crystal growth-based technologies" project (GA No. MAB/2020/14) carried out within the International Research Agendas programme of the Foundation for Polish Science co-financed by the European Union under the European Regional Development Fund and the European Union's Horizon 2020 research and innovation programme Teaming for Excellence (GA. No. 857543) for support of this work. We also gratefully acknowledge Poland's high-performance computing infrastructure PLGrid (HPC Centers: ACK Cyfronet AGH) for providing computer facilities and support within computational (grant no. PLG/2024/017110) and for awarding this project access to the LUMI supercomputer, owned by the EuroHPC Joint Undertaking, hosted by CSC (Finland) and the LUMI consortium through (grant no. PLL/2023/4/016319). The work in China is supported by Starting Research Fund of Qingyuan Innovation Laboratory (00524009).

Conflicts of interest

All authors declared that there are no conflicts of interest.

Ethical approval and consent to participate

Not applicable.

Consent for publication

Not applicable.

REFERENCES

1. Kittel, C. In *Kittel's Introduction to Solid State Physics, Global Edition*, 8th ed.; Introduction to solid state physics; John Wiley & Sons, 2021. pp 1-24. Available from: https://www.wiley.com/en-ie/Kittel's+Introduction+to+Solid+State+Physics%2C+Global+Edition%2C+8th+Edition-p-9781119454168 (accessed 2025-02-25).
2. Crawford, J.H.; Slifkin, L.M. *Point Defects in Solids: General and Ionic Crystals*; Springer US, 2013. DOI
3. Mosquera-Lois, I.; Kavanagh, S. R.; Klarbring, J.; Tolborg, K.; Walsh, A. Imperfections are not 0 K: free energy of point defects in crystals. *Chem. Soc. Rev.* **2023**, *52*, 5812-26. DOI PubMed
4. Walsh, A.; Zunger, A. Instilling defect tolerance in new compounds. *Nat. Mater.* **2017**, Online ahead of print. DOI PubMed
5. Buckeridge, J. Equilibrium point defect and charge carrier concentrations in a material determined through calculation of the self-consistent Fermi energy. *Comput. Phys. Commun.* **2019**, *244*, 329-42. DOI
6. Zunger, A.; Malyi, O. I. Understanding doping of quantum materials. *Chem. Rev.* **2021**, *121*, 3031-60. DOI PubMed

7. Goyal, A.; Gorai, P.; Toberer, E. S.; Stevanović, V. First-principles calculation of intrinsic defect chemistry and self-doping in PbTe. *npj. Comput. Mater.* **2017**, *3*, 47. DOI
8. Broberg, D.; Bystrom, K.; Srivastava, S.; et al. High-throughput calculations of charged point defect properties with semi-local density functional theory - performance benchmarks for materials screening applications. *npj. Comput. Mater.* **2023**, *9*, 1015. DOI
9. Van de Walle, C.G.; Neugebauer, J. First-principles calculations for defects and impurities: applications to III-nitrides. *J. Appl. Phys.* **2004**, *95*, 3851-79. DOI
10. Freysoldt, C.; Grabowski, B.; Hickel, T.; et al. First-principles calculations for point defects in solids. *Rev. Mod. Phys.* **2014**, *86*, 253-305. DOI
11. Zunger, A. Practical doping principles. *Appl. Phys. Lett.* **2003**, *83*, 57-9. DOI
12. Liu, Q.; Dalpian, G. M.; Zunger, A. Antidoping in insulators and semiconductors having intermediate bands with trapped carriers. *Phys. Rev. Lett.* **2019**, *122*, 106403. DOI PubMed
13. Zhang, S.; Wei, S.; Zunger, A. Overcoming doping bottlenecks in semiconductors and wide-gap materials. *Physica. B.* **1999**, *273-274*, 976-80. DOI
14. Kılıç, Ç.; Zunger, A. *n* -type doping of oxides by hydrogen. *Appl. Phys. Lett.* **2002**, *81*, 73-5. DOI
15. Van de Walle, C.G.; Neugebauer, J. Universal alignment of hydrogen levels in semiconductors, insulators and solutions. *Nature* **2003**, *423*, 626-8. DOI PubMed
16. Yu, Y. G.; Zhang, X.; Zunger, A. Natural off-stoichiometry causes carrier doping in half-Heusler filled tetrahedral structures. *Phys. Rev. B.* **2017**, *95*, 085201. DOI
17. Alkauskas, A.; Mccluskey, M. D.; Van de Walle, C. G. Tutorial: defects in semiconductors - combining experiment and theory. *J. Appl. Phys.* **2016**, *119*, 181101. DOI
18. Vashist, L.; Gopidi, H. R.; Khan, M. R.; Malyi, O. I. Noble gas functional defect with unusual relaxation pattern in solids. *J. Phys. Chem. Lett.* **2023**, *14*, 9090-5. DOI PubMed
19. Choi, J.; Na, K.; Lee, S.; Hwang, C. S. First-principles study on the formation of a vacancy in Ge under biaxial compressive strain. *Thin. Solid. Films.* **2010**, *518*, 6373-7. DOI
20. Komsa, H.; Rantala, T. T.; Pasquarello, A. Finite-size supercell correction schemes for charged defect calculations. *Phys. Rev. B.* **2012**, *86*, 045112. DOI
21. Freysoldt, C.; Neugebauer, J.; Van de Walle, C. G. Electrostatic interactions between charged defects in supercells. *Phys. Status. Solidi. (b).* **2011**, *248*, 1067-76. DOI
22. Freysoldt, C.; Neugebauer, J.; Van de Walle, C. G. Fully ab initio finite-size corrections for charged-defect supercell calculations. *Phys. Rev. Lett.* **2009**, *102*, 016402. DOI PubMed
23. Makov, G.; Payne, M. C. Periodic boundary conditions in ab initio calculations. *Phys. Rev. B. Condens. Matter.* **1995**, *51*, 4014-22. DOI PubMed
24. Gopidi, H. R.; Vashist, L.; Malyi, O. I. Physics of band-filling correction in defect calculations of solid-state materials. *RSC. Adv.* **2024**, *14*, 17675-83. DOI PubMed PMC
25. Sopiha, K. V.; Malyi, O. I.; Persson, C.; Wu, P. Chemistry of oxygen ionosorption on SnO_2 surfaces. *ACS. Appl. Mater. Interfaces.* **2021**, *13*, 33664-76. DOI PubMed PMC
26. Lany, S.; Zunger, A. Assessment of correction methods for the band-gap problem and for finite-size effects in supercell defect calculations: case studies for ZnO and GaAs. *Phys. Rev. B.* **2008**, *78*, 235104. DOI
27. Castleton, C. W. M.; Mirbt, S. Finite-size scaling as a cure for supercell approximation errors in calculations of neutral native defects in InP. *Phys. Rev. B.* **2004**, *70*, 195202. DOI
28. Muy, S.; Johnston, C.; Marzari, N. AiiDA-defects: an automated and fully reproducible workflow for the complete characterization of defect chemistry in functional materials. *Electron. Struct.* **2023**, *5*, 024009. DOI
29. Goyal, A.; Gorai, P.; Peng, H.; Lany, S.; Stevanović, V. A computational framework for automation of point defect calculations. *Comput. Mater. Sci.* **2017**, *130*, 1-9. DOI
30. Broberg, D.; Medasani, B.; Zimmermann, N. E.; et al. PyCDT: A Python toolkit for modeling point defects in semiconductors and insulators. *Comput. Phys. Commun.* **2018**, *226*, 165-79. DOI
31. Xiao, J.; Yang, K.; Guo, D.; et al. Realistic dimension-independent approach for charged-defect calculations in semiconductors. *Phys. Rev. B.* **2020**, *101*, 165306. DOI
32. Chen, W.; Pasquarello, A. First-principles determination of defect energy levels through hybrid density functionals and GW. *J. Phys. Condens. Matter.* **2015**, *27*, 133202. DOI PubMed
33. Janotti, A.; Van de Walle, C. G. Oxygen vacancies in ZnO. *Appl. Phys. Lett.* **2005**, *87*, 122102. DOI
34. Thiering, G.; Gali, A. *Ab Initio* magneto-optical spectrum of group-IV vacancy color centers in diamond. *Phys. Rev. X.* **2018**, *8*, 021063. DOI
35. Li, S.; Chou, J.; Hu, A.; et al. Giant shift upon strain on the fluorescence spectrum of V_NN_B color centers in *h*-BN. *npj. Quantum. Inf.* **2020**, *6*, 312. DOI
36. Abdi, M.; Chou, J.; Gali, A.; Plenio, M. B. Color centers in hexagonal boron nitride monolayers: a group theory and Ab initio analysis. *ACS. Photonics.* **2018**, *5*, 1967-76. DOI
37. Alkauskas, A.; Broqvist, P.; Pasquarello, A. Defect energy levels in density functional calculations: alignment and band gap problem. *Phys. Rev. Lett.* **2008**, *101*, 046405. DOI PubMed

38. Malyi, O. I.; Yeung, M. T.; Poeppelmeier, K. R.; Persson, C.; Zunger, A. Spontaneous non-stoichiometry and ordering in degenerate but gapped transparent conductors. *Matter* **2019**, *1*, 280-94. DOI
39. Xu, X.; Randorn, C.; Efstathiou, P.; Irvine, J. T. A red metallic oxide photocatalyst. *Nat. Mater.* **2012**, *11*, 595-8. DOI PubMed
40. Cheikh, D.; Hogan, B. E.; Vo, T.; et al. Praseodymium telluride: a high-temperature, high-ZT thermoelectric material. *Joule* **2018**, *2*, 698-709. DOI
41. Dismukes, J. P.; White, J. G. The preparation, properties, and crystal structures of some scandium sulfides in the range Sc_2S_3-ScS. *Inorg. Chem.* **1964**, *3*, 1220-8. DOI
42. Male, J. P.; Hogan, B.; Wood, M.; Cheikh, D.; Snyder, G. J.; Bux, S. K. Using vacancies to tune mechanical and elastic properties in $La_{3-x}Te_4$, $Nd_{3-x}Te_4$, and $Pr_{3-x}Te_4$ rare earth telluride thermoelectric materials. *Mater. Today. Phys.* **2023**, *32*, 101016. DOI
43. Wickramaratne, D.; Dreyer, C. E.; Monserrat, B.; et al. Defect identification based on first-principles calculations for deep level transient spectroscopy. *Appl. Phys. Lett.* **2018**, *113*, 192106. DOI
44. Castelletto, S.; Johnson, B. C.; Ivády, V.; et al. A silicon carbide room-temperature single-photon source. *Nat. Mater.* **2014**, *13*, 151-6. DOI PubMed
45. Kresse, G.; Hafner, J. Ab initio molecular dynamics for liquid metals. *Phys. Rev. B. Condens. Matter.* **1993**, *47*, 558-61. DOI PubMed
46. Kresse, G.; Hafner, J. Ab initio molecular-dynamics simulation of the liquid-metal-amorphous-semiconductor transition in germanium. *Phys. Rev. B. Condens. Matter.* **1994**, *49*, 14251-69. DOI PubMed
47. Kresse, G.; Furthmüller, J. Efficiency of ab-initio total energy calculations for metals and semiconductors using a plane-wave basis set. *Comput. Mater. Sci.* **1996**, *6*, 15-50. DOI
48. Kresse, G.; Furthmüller, J. Efficient iterative schemes for ab initio total-energy calculations using a plane-wave basis set. *Phys. Rev. B. Condens. Matter.* **1996**, *54*, 11169-86. DOI PubMed
49. Perdew, J. P.; Burke, K.; Ernzerhof, M. Generalized gradient approximation made simple. *Phys. Rev. Lett.* **1996**, *77*, 3865-8. DOI PubMed
50. Ong, S. P.; Richards, W. D.; Jain, A.; et al. Python materials genomics (pymatgen): a robust, open-source python library for materials analysis. *Comput. Mater. Sci.* **2013**, *68*, 314-9. DOI
51. Momma, K.; Izumi, F. *VESTA 3* for three-dimensional visualization of crystal, volumetric and morphology data. *J. Appl. Cryst.* **2011**, *44*, 1272-6. DOI
52. Bragg, W. L. XLII. *The. crystalline. structure. of. copper.28*, 355-60. DOI
53. Hull, A. W.; Davey, W. P. Graphical determination of hexagonal and tetragonal crystal structures from X-ray data. *Phys. Rev.* **1921**, *17*, 549-70. DOI
54. Hannerz, H.; Svensson, G.; Istomin, S.; D'yachenko, O. Transmission electron microscopy and neutron powder diffraction studies of $GdFeO_3$ type $SrNbO_3$. *J. Solid. State. Chem.* **1999**, *147*, 421-8. DOI
55. Matsuishi, S.; Nomura, T.; Hirano, M.; Kodama, K.; Shamoto, S.; Hosono, H. Direct synthesis of powdery inorganic electride $[Ca_{24}Al_{28}O_{64}]^{4+}(e^-)_4$ and determination of oxygen stoichiometry. *Chem. Mater.* **2009**, *21*, 2589-91. DOI
56. Schneider, S. B.; Frankovsky, R.; Schnick, W. Synthesis of alkaline earth diazenides $M_{AE}N_2$ (M_{AE} = Ca, Sr, Ba) by controlled thermal decomposition of azides under high pressure. *Inorg. Chem.* **2012**, *51*, 2366-73. DOI PubMed
57. Odaka HO, Yuzo Shigesato YS, Takashi Murakami TM, Shuichi Iwata SI. Electronic structure analyses of Sn-doped In_2O_3. *Jpn. J. Appl. Phys.* **2001**, *40*, 3231. DOI
58. Setyawan, W.; Curtarolo, S. High-throughput electronic band structure calculations: challenges and tools. *Comput. Mater. Sci.* **2010**, *49*, 299-312. DOI
59. Chan, M. K.; Ceder, G. Efficient band gap prediction for solids. *Phys. Rev. Lett.* **2010**, *105*, 196403. DOI PubMed
60. He, J.; Baldassarri, B.; Wolverton, C. Assessment of exchange-correlation functionals on oxygen vacancy formation energies of metal oxides. *Phys. Rev. B.* **2023**, *108*, 104103. DOI
61. Nazarov, R.; Hickel, T.; Neugebauer, J. Vacancy formation energies in fcc metals: influence of exchange-correlation functionals and correction schemes. *Phys. Rev. B.* **2012**, *85*, 144118. DOI
62. Jain, A.; Ong, S. P.; Hautier, G.; et al. Commentary: the materials project: a materials genome approach to accelerating materials innovation. *APL. Materials.* **2013**, *1*, 011002. DOI
63. Zhang, X.; Zhang, L.; Perkins, J. D.; Zunger, A. Intrinsic transparent conductors without doping. *Phys. Rev. Lett.* **2015**, *115*, 176602. DOI PubMed
64. Ricci, F.; Dunn, A.; Jain, A.; Rignanese, G.; Hautier, G. Gapped metals as thermoelectric materials revealed by high-throughput screening. *J. Mater. Chem. A.* **2020**, *8*, 17579-94. DOI
65. Burton, L. A.; Ricci, F.; Chen, W.; Rignanese, G.; Hautier, G. High-throughput identification of electrides from all known inorganic materials. *Chem. Mater.* **2018**, *30*, 7521-6. DOI
66. Kim, S. W.; Shimoyama, T.; Hosono, H. Solvated electrons in high-temperature melts and glasses of the room-temperature stable electride $[Ca_{24}Al_{28}O_{64}]^{4+}\cdot 4e^-$. *Science* **2011**, *333*, 71-4. DOI PubMed
67. Matsuishi, S.; Toda, Y.; Miyakawa, M.; et al. High-density electron anions in a nanoporous single crystal: $[Ca_{24}Al_{28}O_{64}]^{4+}(4e^-)$. *Science* **2003**, *301*, 626-9. DOI PubMed
68. Hosono, H.; Kitano, M. Advances in materials and applications of inorganic electrides. *Chem. Rev.* **2021**, *121*, 3121-85. DOI PubMed
69. Li, G.; Aydemir, U.; Wood, M.; et al. Mechanical properties of thermoelectric lanthanum telluride from quantum mechanics. *J. Phys. D:. Appl. Phys.* **2017**, *50*, 274002. DOI

70. Hu, X.; Wu, Z.; Li, Z.; et al. High-throughput search for lossless metals. *Phys. Rev. Mater.* **2022**, *6*, 065203. DOI
71. Khan, M. R.; Gopidi, H. R.; Malyi, O. I. Optical properties and electronic structures of intrinsic gapped metals: inverse materials design principles for transparent conductors. *Appl. Phys. Lett.* **2023**, *123*, 061101. DOI
72. Zhang, L.; Zhou, Y.; Guo, L.; et al. Correlated metals as transparent conductors. *Nat. Mater.* **2016**, *15*, 204-10. DOI PubMed
73. Walsh, A.; Sokol, A. A.; Buckeridge, J.; Scanlon, D. O.; Catlow, C. R. A. Oxidation states and ionicity. *Nat. Mater.* **2018**, *17*, 958-64. DOI PubMed
74. Walsh, A.; Sokol, A. A.; Buckeridge, J.; Scanlon, D. O.; Catlow, C. R. A. Electron counting in solids: oxidation states, partial charges, and ionicity. *J. Phys. Chem. Lett.* **2017**, *8*, 2074-5. DOI PubMed
75. Malyi, O. I.; Dalpian, G. M.; Zhao, X. G.; Wang, Z.; Zunger, A. Realization of predicted exotic materials: the burden of proof. *Mater. Today.* **2020**, *32*, 35-45. DOI
76. Malyi, O. I.; Zunger, A. False metals, real insulators, and degenerate gapped metals. *Appl. Phys. Rev.* **2020**, *7*, 041310. DOI
77. Khan, M. R.; Gopidi, H. R.; Wlazło, M.; Malyi, O. I. Fermi-level instability as a way to tailor the properties of La_3Te_4. *J. Phys. Chem. Lett.* **2023**, *14*, 1962-7. DOI PubMed
78. Hart, G. L.; Zunger, A. Origins of nonstoichiometry and vacancy ordering in $Sc_{1-x}\square_xS$. *Phys. Rev. Lett.* **2001**, *87*, 275508. DOI PubMed
79. Li, B.; Mudring, A. V.; Corbett, J. D. Valence compounds versus metals. Synthesis, characterization, and electronic structures of cubic Ae_4Pn_3 phases in the systems Ae = Ca, Sr, Ba, Eu; Pn = As, Sb, Bi. *Inorg. Chem.* **2003**, *42*, 6940-5. DOI PubMed